Clusters and Superclusters of Galaxies

Neta A. Bahcall
Princeton University Observatory
Princeton, NJ 08544

ABSTRACT

Rich clusters of galaxies are the most massive virialized systems known. Even though they contain only a small fraction of all galaxies, rich clusters provide a powerful tool for the study of galaxy formation, dark matter, large-scale structure, and cosmology.

Superclusters, the largest known systems of galaxies, extend to $\sim 100h^{-1}$ Mpc in size and highlight the large-scale structure of the universe. This large-scale structure reflects initial conditions in the early universe and places strong contraints on models of galaxy formation and on cosmology.

Some of the questions that can be addressed with clusters and superclusters of galaxies include: How did galaxies and larger structures form and evolve? What is the amount, composition, and distribution of matter in clusters and larger structures? How does the cluster mass density relate to the matter density in the universe? What constraints can the cluster and supercluster data place on cosmology?

I will discuss in these lectures some of the properties of clusters and superclusters of galaxies that can be used to investigate these topics.

1. Introduction

Clusters and superclusters of galaxies have been studied extensively both for their intrinsic properties and to investigate the dark matter in the universe, the baryon content of the universe, large-scale structure, evolution, and cosmology. For previous reviews see Zwicky (1958), Bahcall (1977, 1988, 1996), Oort (1983), Dressler (1984), Rood (1988), and Peebles (1993).

In these lectures I discuss the following topics and their implications for structure formation and cosmology.

Section 2: Optical properties of galaxy clusters

Section 3: X-ray properties of galaxy clusters

Section 4: The baryon fraction in clusters

Section 5: Cluster masses

Section 6: Where is the dark matter?

Section 7: The mass function of clusters

Section 8: Quasar-cluster association

Section 9: Superclusters

Section 10: The cluster correlation function

Section 11: Peculiar motions of clusters

Section 12: Some unsolved problems

A Hubble constant of $H_o = 100h$ km s^{-1} Mpc^{-1} is used throughout.

2. Optical Properties of Galaxy Clusters

2.1. Typical Properties of Clusters and Groups

Clusters of galaxies are bound, virialized, high overdensity systems of galaxies, held together by the clusters self gravity. Rich clusters contain, by traditional definition (Abell 1958), at least 30 galaxies brighter than $m_3 + 2^m$ (where m_3 is the magnitude of the third brightest cluster member) within a radius of $R \simeq 1.5h^{-1}$ Mpc of the cluster center. This galaxy count is generally defined as the richness of the cluster. The galaxies in rich clusters move with random peculiar velocities of typically ~ 750 km s^{-1} (median line-of-sight velocity dispersion). This motion corresponds to a typical rich cluster mass (within $1.5h^{-1}$ Mpc) of $\sim 5 \times 10^{14} h^{-1}\ M_\odot$. In addition to galaxies, all rich clusters contain an intracluster medium of hot plasma, extending as far as the main galaxy concentration ($R \sim 1.5h^{-1}$ Mpc). The typical temperature of the hot intracluster gas is ~ 5 kev, with a range from ~ 2 to 14 kev; the central gas density is $\sim 10^{-3}$ electrons cm^{-3}. The hot plasma is detected through the luminous X-ray emission it produces by thermal bremsstrahlung radiation, with $L_x \sim 10^{44}$ erg s^{-1}.

Like mountain peaks on earth, the high density rich clusters are relatively "rare" objects; they exhibit a spatial number density of $\sim 10^{-5}$ clusters Mpc^{-3}, as compared with $\sim 10^{-2}$ galaxies Mpc^{-3} for the density of bright galaxies.

The main properties of clusters and groups of galaxies are summarized in Table 1 (Bahcall 1996). The table lists the typical range and/or median value of each observed property. Groups and poor clusters, whose properties are also listed, provide a natural and continuous extension to lower richness, mass, size, and luminosity from the rich and rare clusters.

In the following subsections I discuss in more detail some of these intrinsic cluster properties.

2.2. Distribution of Clusters with Richness and Distance

An illustration of the distribution of rich clusters with richness and distance is summarized in Table 2. The table refers to the statistical sample of the Abell (1958) cluster catalog (i.e., richness class $R \geq 1$, corresponding to a richness threshold count of $N_R \geq 50$ galaxies within $1.5h^{-1}$ Mpc radius and magnitude $m \leq m_3 + 2^m$ (see Table 1); redshift range $z \simeq 0.02$ to 0.2; and sky coverage $\delta > -27^\circ$ and $|b| \gtrsim 30^\circ$). The Abell catalog covers $\sim 1/3$ of the entire sky to $z \lesssim 0.2$. Recent smaller automated surveys from digitized plates are reported by the Edinburgh-Durham catalog (EDCC; Lumsden et al. 1992), and the APM survey (Dalton et al. 1992). A large automated cluster catalog will be available in the near future from the Sloan Digital Sky Survey (SDSS). This and other planned surveys will allow a more accurate determination of the distribution of rich clusters with richness and distance and other statistical studies of clusters.

2.3. Number Density of Clusters

The number density of clusters is a strong function of cluster richness. Integrated cluster densities, n_c ($> N_R$), representing the number density of clusters above a given richness threshold, and the associated mean cluster separation, d ($\equiv n_c^{-1/3}$), are listed in Table 3 (Bahcall and Cen 1993).

Table 1: Typical Properties of Clusters and Groups.

Property[a]	Rich clusters	Groups and poor clusters
Richness[b]	30–300 galaxies	3–30 galaxies
Radius[c]	(1–2) h^{-1} Mpc	(0.1–1) h^{-1} Mpc
Radial velocity dispersion[d]	400–1400 km s^{-1}	100–500 km s^{-1}
Radial velocity dispersion[d] (median)	~ 750 km s^{-1}	~ 250 km s^{-1}
Mass ($r \leq 1.5h^{-1}$ Mpc)[e]	$(10^{14}$–$2\times10^{15})h^{-1}$ $\mathcal{M}_\odot$	$(10^{12.5}$–$10^{14})h^{-1}$ $\mathcal{M}_\odot$
Luminosity (B)[f] ($r \leq 1.5h^{-1}$ Mpc)	$(6\times10^{11}$–$6\times10^{12})h^{-2}$ $L_\odot$	$(10^{10.5}$–$10^{12})h^{-2}$ $L_\odot$
$\langle\mathcal{M}/L_{\rm B}\rangle$[g]	$\sim 300h$ $\mathcal{M}_\odot/L_\odot$	$\sim 200h$ $\mathcal{M}_\odot/L_\odot$
X-ray temperature[h]	2–14 keV	$\lesssim 2$ keV
X-ray luminosity[h]	$(10^{42.5}$–$10^{45})h^{-2}$ erg s^{-1}	$\lesssim 10^{43}h^{-2}$ erg s^{-1}
Cluster number density[i]	$(10^{-5}$–$10^{-6})h^3$ Mpc^{-3}	$(10^{-3}$–$10^{-5})h^3$ Mpc^{-3}
Cluster correlation scale[j]	$(22\pm4)h^{-1}$ Mpc ($R \geq 1$)	$(13\pm2)h^{-1}$ Mpc
Fraction of galaxies in clusters or groups[k]	$\sim 5\%$	$\sim 55\%$

[a] In most entries, the typical range in the listed property or the median value is given. Groups and poor clusters are a natural and continuous extension to lower richness, mass, size, and luminosity from the rich and rare clusters.

[b] Cluster richness: the number of cluster galaxies brighter than $m_3 + 2^m$ (where m_3 is the magnitude of the third brightest cluster galaxy), and located within a $1.5h^{-1}$ Mpc radius of the cluster center (§2.2).

[c] The radius of the main concentration of galaxies (where, typically, the galaxy surface density drops to $\sim 1\%$ of the central core density). Many clusters and groups are embedded in larger scale structures (to tens of Mpc).

[d] Typical observed range and median value for the radial (line-of-sight) velocity dispersion in groups and clusters (§2.9).

[e] Dynamical mass range of clusters within $1.5h^{-1}$ Mpc radius (§2.10).

Table 2: Distribution of Abell Clusters with Distance and Richness.[a]

Distance distribution			Richness distribution		
D	$\langle z_{\rm est}\rangle$	$N_{\rm cl}(R \geq 1)$	R	N_R	$N_{\rm cl}$
1	0.0283	9	(0)[b]	(30–49)	($\sim 10^3$)
2	0.0400	2	1	50–79	1224
3	0.0577	33	2	80–129	383
4	0.0787	60	3	130–199	68
5	0.131	657	4	200–299	6
6	0.198	921	5	≥ 300	1
	Total	1682		Total ($R \geq 1$)	1682

Nearby redshift sample[c,d] $D \leq 4$	Distant projected sample[d] $D = 5 + 6$
$N_{\rm cl}$(total)	104	1574
$N_{\rm cl}(b \geq 30°)$	71	984
$N_{\rm cl}(b \leq -30°)$	33	563
$N_{\rm cl}(R = 1)$	82	1125
$N_{\rm cl}(R \geq 2)$	22	422

[a] Statistical sample. $|b|$ boundaries as given in Table 1 of Abell (1958). Notation: D = distance group (defined by the estimated redshifts of the clusters); $\langle z_{\rm est}\rangle$ = average estimated redshift from the magnitude of the tenth brightest galaxy; $N_{\rm cl}$ = number of clusters; R = richness class; N_R = number of galaxies brighter than $m_3 + 2^m$ within $R_A = 1.5h^{-1}$ Mpc (richness count).

[b] $R = 0$ clusters are not part of the statistical sample.

[c] Redshifts by Hoessel et al. (1980).

[d] This sample is limited to $|b| \geq 30°$ in addition to the $|b|$ boundaries of the statistical sample.

2.4. Fraction of Galaxies in Clusters

The fraction of galaxies in rich $R \gtrsim 0$ clusters is $\sim 5\%$ (within the Abell radius $R_A = 1.5h^{-1}$ Mpc). The fraction of all galaxies that belong in clusters increases with increasing radius R_A and with decreasing cluster richness threshold.

The average number of galaxies per cluster for $R \geq 0$ clusters within $1.5h^{-1}$ Mpc radius and $m \leq m_3 + 2^m$ is $\langle N_R \rangle_{\rm median} \simeq 50$, or $\langle N_R \rangle_{\rm mean} \simeq 56$. For $R \geq 1$ clusters the average is $\langle N_R \rangle_{\rm median} \simeq 60$, or $\langle N_R \rangle_{\rm mean} \simeq 75$. The number of galaxies increases to fainter luminosities following the Schechter (1976) luminosity function.

2.5. Galaxy Overdensity in Rich Clusters

The average number density of bright ($\gtrsim L^{*)}$ galaxies in $R \gtrsim 0$ clusters (within $R_A = 1.5h^{-1}$ Mpc) is

$$n_g({\rm cluster}) \sim 3h^3 \ {\rm galaxies\ Mpc}^{-3}. \tag{1}$$

The average overall (field) number density of bright ($\gtrsim L^*$) galaxies is

$$n_g({\rm field}) \sim 1.5 \times 10^{-2} h^3 \ {\rm galaxies\ Mpc}^{-3}. \tag{2}$$

The average galaxy overdensity in rich ($R \geq 0$) clusters (within $1.5h^{-1}$ Mpc radius) is thus

$$n_g({\rm cluster})/n_g({\rm field}) \sim 200. \tag{3}$$

The typical threshold galaxy overdensity in clusters (within $1.5h^{-1}$ Mpc radius) is

$$R \geq 0 \ {\rm clusters}: \ \ n_g({\rm cluster})/n_g({\rm field}) \gtrsim 100, \tag{4}$$

Table 3: Number Density of Clusters.

R	N_R	$n_c\ (>N_R)h^3$ (Mpc^{-3})[a]	$d\ (>N_R)h^{-1}$ (Mpc)
≥ 0	≥ 30	13.5×10^{-6}	42
≥ 1	≥ 50	6.0×10^{-6}	55
≥ 2	≥ 80	1.2×10^{-6}	94
≥ 3	≥ 130	1.5×10^{-7}	188

[a] Approximate uncertainties are $10^{\pm 0.2}$ for the $R \geq 0, 1, 2$ densities and $10^{\pm 0.3}$ for $R \geq 3$.

$$R \geq 1 \text{ clusters}: \quad n_g(\text{cluster})/n_g(\text{field}) \gtrsim 200. \tag{5}$$

The galaxy overdensity increases at smaller radii from the cluster center. The galaxy overdensity in the cores of typical compact rich clusters is approximately

$$n_g^0(\text{cluster core})/n_g(\text{field}) \sim 10^4 - 10^5. \tag{6}$$

2.6. Density Profile

The radial density distribution of galaxies in a rich cluster can be approximated by a bounded Emden isothermal profile (Zwicky 1957; Bahcall 1977), or by its King approximation (King 1972) in the *central* regions.

In the central regions, the King approximation for the galaxy distribution is

$$n_g(r) = n_g^0(1 + r^2/R_c^2)^{-3/2}, \quad \text{spatial profile} \tag{7}$$

$$S_g(r) = S_g^0(1 + r^2/R_c^2)^{-1}, \quad \text{projected profile.} \tag{8}$$

$n_g(r)$ and $S_g(r)$ are, respectively, the space and projected profiles (of the number density of galaxies, or brightness), n_g^0 and S_g^0 are the respective central densities, and R_c is the cluster core radius [where $S(R_c) = S^0/2$]. Typical central densities and core radii of clusters are listed in the following subsection. The projected and space central densities relate as

$$S_g^0 = 2R_c n_g^0. \tag{9}$$

A bounded Emden isothermal profile of galaxies in clusters yields a profile slope that varies approximately as (Bahcall 1977)

$$S_g(r \lesssim R_c/3) \sim \text{constant}, \tag{10}$$

$$S_g(R_c \lesssim r \lesssim 10R_c) \propto r^{-1.6}; \tag{11}$$

therefore

$$n_g(R_c \lesssim r \lesssim 10R_c) \propto r^{-2.6}. \tag{12}$$

The galaxy–cluster cross-correlation function (Peebles 1980; Lilje and Efstathiou 1988) also represents the average radial density distribution of galaxies around clusters. For $R \geq 1$ clusters, and r in h^{-1} Mpc, these references suggest, respectively

$$\xi_{gc}(r) \simeq 130r^{-2.5} + 70r^{-1.7} \tag{13}$$

or

$$\xi_{gc}(r) \simeq 120r^{-2.2} \ . \tag{14}$$

The average density distribution profile of galaxies in clusters thus follows, approximately,

$$n_g(r) \propto r^{-2.4\pm0.2} \quad \text{(spatial)}, \quad r > R_c \tag{15}$$

$$S_g(r) \propto r^{-1.4\pm0.2} \quad \text{(projected)}, \quad r > R_c \ . \tag{16}$$

Some substructure (subclumping) in the distribution of galaxies exists in a significant fraction of rich clusters ($\sim 40\%$) (Geller 1990).

2.7. Central Density and Core Size

Central number density of galaxies in rich compact clusters (Bahcall 1975, 1977; Dressler 1978) is (for galaxies in the brightest 3 magnitude range)

$$n_g^0(\Delta m \simeq 3^m) \sim 10^3 h^3 \text{ galaxies Mpc}^{-3}. \tag{17}$$

The central density reaches $\sim 10^4 h^3$ galaxies Mpc^{-3} for the richest compact clusters. The typical central *mass* density in rich compact clusters, determined from cluster dynamics is

$$\begin{aligned} \rho_0(\text{mass}) &\simeq 9\sigma_{r,c}^2/4\pi G R_c^2 \\ &\sim 4\times 10^{15}\mathcal{M}_\odot \text{ Mpc}^{-3}[(\sigma_{r,c}/10^3 \text{ km s}^{-1})/(R_c/0.2 \text{ Mpc})]^2 h^2 \end{aligned} \tag{18}$$

where $\sigma_{r,c}$ is the radial (line-of-sight) central cluster velocity dispersion (in km s^{-1}) and R_c is the cluster core radius (in Mpc).

Core radii of typical rich compact clusters, determined from the galaxy distribution (Bahcall 1975; Dressler 1978; Sarazin 1986) are in the range

$$R_c \simeq (0.1 - 0.25) h^{-1} \text{ Mpc} \tag{19}$$

Core radii of the X-ray emitting intracluster gas (§3) are

$$R_c(\text{X} - \text{rays}) \simeq (0.1 - 0.3) h^{-1} \text{ Mpc} \tag{20}$$

The core radius of the mass distribution determined from gravitational lensing observations of some clusters may be smaller, $R_c \lesssim 50$ kpc, than determined by the galaxy and gas distribution.

The typical central density of the hot intracluster gas in rich clusters (§3) is

$$n_e \sim 10^{-3} \text{ electrons cm}^{-3}. \tag{21}$$

2.8. Galactic Content in Rich Clusters

The fraction of elliptical, S0, and spiral galaxies in rich clusters differs from that in the field, and depends on the classification type, or density, of the cluster (see §2.11) (Bahcall 1977; Oemler 1974; Dressler 1980). See Table 4.

The fraction of elliptical (E) and S0 galaxies increases and the fraction of spirals decreases toward the central cores of rich compact clusters. The fraction of spiral galaxies in the dense cores of some rich clusters (e.g., the Coma cluster) may be close to zero.

The galactic content of clusters as represented in Table 4 is part of the general density–morphology relation of galaxies (Dressler 1980; Postman and Geller 1984); as the local density of galaxies increases, the fraction of E and S0 galaxies increases and the fraction of spirals decreases. For local galaxy densities $n_g \lesssim 5$ galaxies Mpc^{-3}, the fractions remain approximately constant at the average "Field" fractions listed above.

2.9. Velocity Dispersion

The typical radial (line-of-sight) velocity dispersion of galaxies in rich clusters (median value) is

$$\sigma_r \sim 750 \ \mathrm{km\,s^{-1}}. \tag{22}$$

The typical range of radial velocity dispersion in rich clusters (Struble and Rood 1991) is

$$\sigma_r \sim 400\text{–}1400 \ \mathrm{km\,s^{-1}}. \tag{23}$$

A weak correlation between σ_r and richness exists; richer clusters exhibit, on average, larger velocity dispersion (Bahcall 1981). The observed velocity dispersion of galaxies in rich clusters is generally consistent with the velocity implied by the X-ray temperature of the hot

Table 4: Typical Galactic Content of Clusters ($r \lesssim 1.5h^{-1}$ Mpc).

Cluster type	E	S0	Sp	(E+S0)/Sp
Regular clusters (cD)	35%	45%	20%	4.0
Intermediate clusters (spiral-poor)	20%	50%	30%	2.3
Irregular clusters (spiral-rich)	15%	35%	50%	1.0
Field	10%	20%	70%	0.5

intracluster gas (§3.5), as well as with the cluster velocity dispersion implied from observations of gravitational lensing by clusters (except possibly in the central core). Velocity dispersion and temperature profiles as a function of distance from the cluster center have been measured only for a small number of clusters so far. The profiles are typically isothermal $[\sigma_r^2(r) \sim T_{\rm x}(r) \sim \text{constant}]$ for $r \lesssim 0.5 - 1h^{-1}$ Mpc, and drop somewhat at larger distances.

2.10. Mass, Luminosity, and Mass-to-Luminosity Ratio

The typical dynamical mass of rich clusters within $1.5h^{-1}$ Mpc radius sphere (determined from the virial theorem for an isothermal distribution) is

$$\mathcal{M}_{\rm cl}(\leq 1.5) \simeq \frac{2\sigma_r^2(1.5h^{-1}\ {\rm Mpc})}{G} \simeq 0.7 \times 10^{15} \left(\frac{\sigma_r}{1000}\right)^2 \simeq 0.4 \times 10^{15} h^{-1} \mathcal{M}_\odot \ (\text{for } \sigma_r \sim 750\ {\rm km\,s^{-1}}). \tag{24}$$

The approximate range of masses for $R \gtrsim 0$ clusters (within $1.5h^{-1}$ Mpc) is

$$\mathcal{M}_{\rm cl}(\leq 1.5) \sim (0.1\text{–}2) \times 10^{15} h^{-1}\ \mathcal{M}_\odot. \tag{25}$$

Comparable masses are obtained using the X-ray temperature and distribution of the hot intracluster gas (Hughes 1989; Bahcall and Cen 1993; Lubin and Bahcall 1993; §3).

The typical (median) blue luminosity of rich clusters (within $1.5h^{-1}$ Mpc) is

$$L_{\rm cl}(\leq 1.5) \sim 10^{12} h^{-2}\ L_\odot \tag{26}$$

The approximate range of rich cluster blue luminosities is

$$L_{\rm cl}(\leq 1.5) \sim (0.6\text{–}6) \times 10^{12} h^{-2} L_\odot \tag{27}$$

The typical mass-to-luminosity ratio of rich clusters is thus

$$(M/L_B)_{\rm cl} \sim 300h\ (\mathcal{M}_\odot/L_\odot). \tag{28}$$

The inferred mass-density in the universe based on cluster dynamics is

$$\Omega_{\rm dyn} \sim 0.2 \tag{29}$$

(if mass follows light, $M \propto L$, on scales $\gtrsim 1h^{-1}$ Mpc). $\Omega = 1$ corresponds to the critical mass-density needed for a closed universe and $\mathcal{M}/L_B\ (\Omega = 1) \simeq 1500h$.

2.11. Cluster Classification

Rich clusters are classified in a sequence ranging from early- to late-type clusters, or equivalently, from regular to irregular clusters. Many cluster properties (shape, concentration, dominance of brightest galaxy, galactic content, density profile, and radio and X-ray emission) are correlated with position in this sequence. A summary of the sequence and its related properties is given in Table 5. Some specific classification systems include the Bautz–Morgan (BM) System (Bautz and Morgan 1970), which classifies clusters based on the relative contrast (dominance in extent and brightness) of the brightest galaxy to the other galaxies in the cluster, ranging from type I to III in decreasing order of dominance; and the Rood-Sastry (RS) system (Rood and Sastry 1971) which classifies clusters based on the distribution of the ten brightest members (from cD, to binary (B), core (C), line(L), flat (F), and irregular (I)).

3. X-Ray Properties of Galaxy Clusters

3.1. X-Ray Emission from Clusters

All rich clusters of galaxies produce extended X-ray emission due to thermal bremsstrahlung radiation from a hot intracluster gas (Jones and Forman 1984; Sarazin 1986; David et al. 1993; Edge et al. 1990, 1991; Henry et al. 1991, 1992; Burg et al. 1994). The cluster X-ray luminosity emitted in the photon energy band E_1 to E_2 by thermal bremsstrahlung from a hot ($T_{\rm x}$ degrees) intracluster gas of uniform electron density n_e and a radius $R_{\rm x}$ is

$$L_{\rm x} \propto n_e^2 R_{\rm x}^3 T_{\rm x}^{0.5} g(e^{-E_1/kT_{\rm x}} - e^{-E_2/kT_{\rm x}}). \tag{30}$$

The Gaunt factor correction g (of order unity) is a slowly varying function of temperature and energy. The bolometric thermal bremsstrahlung luminosity of a cluster core can be approximated by

$$L_{\rm x}({\rm core}) \simeq 1.4 \times 10^{42} n_e({\rm cm}^{-3})^2 R_c({\rm kpc})^3 kT_{\rm x}({\rm keV})^{0.5} h^{-2}\ {\rm erg\,s}^{-1}. \tag{31}$$

Some of the main properties of the hot intracluster gas are summarized below.

3.2. X-Ray Properties of Clusters

Some of the main properties of the X-ray emission from rich clusters of galaxies are summarized in Table 6.

Table 5: Cluster Classification and Related Characteristics.

Property	Regular (Early) type clusters	Intermediate clusters	Irregular (late) type clusters
Zwicky type	Compact	Medium-compact	Open
BM type	I, I–II, II	(II), II–III	(II–III), III
RS type	cD,B,(L,C)	(L),(F),(C)	(F),I
Shape symmetry	Symmetrical	Intermediate	Irregular shape
Central concentration	High	Moderate	Low
Galactic content	Elliptical-rich	Spiral-poor	Spiral-rich
E fraction	35%	20%	15%
S0 fraction	45%	50%	35%
Sp fraction	20%	30%	50%
E:S0:Sp	3:4:2	2:5:3	1:2:3
Radio emission	$\sim 50\%$ detection	$\sim 50\%$ detection	$\sim 25\%$ detection
X-ray luminosity	High	Intermediate	Low
Fraction of clusters	$\sim 1/3$	$\sim 1/3$	$\sim 1/3$
Examples	A401, Coma	A194	Virgo, A1228

Table 6: X-Ray Properties of Rich Clusters.

Property	Typical value or range	Notes
$L_{\rm x}$ (2–10 keV)	$\sim (10^{42.5}$–$10^{45}) h^{-2}$ erg s^{-1}	a
$I_{\rm x}(r)$	$I_{\rm x}(r) \propto [1+(r/R_c)^2]^{-3\beta+1/2}$	b
$\langle\beta\rangle$	~ 0.7	c
$\rho_{\rm gas}(r)$	$\rho_{\rm gas}(r) \propto [1+(r/R_c)^2]^{-3\beta/2}$	
	$\propto [1+(r/R_c)^2]^{-1}$	d
$kT_{\rm x}$	$\sim$ 2–14 keV	e
$T_{\rm x}$	$\sim 2\times10^7$–10^8 K	e
$\beta_{\rm spect} = \frac{\sigma_r^2}{kT_{\rm x}/\mu m_p}$	~ 1	f
$R_c(x)$	$\sim (0.1$–$0.3) h^{-1}$ Mpc	g
n_e	$\sim 3\times10^{-3} h^{1/2}$ cm^{-3}	h
$\mathcal{M}_{\rm gas}$ ($\lesssim 1.5h^{-1}$ Mpc)	$\sim 10^{13.5}\mathcal{M}_\odot$ [range: $(10^{13}$–$10^{14})\mathcal{M}_\odot$ h$^{-2.5}$]	i
$\mathcal{M}_{\rm gas}/\mathcal{M}_{\rm cl}$ ($\lesssim 1.5h^{-1}$ Mpc)	~ 0.07 (range: 0.03–0.15 h$^{-1.5}$)	i
Iron abundance	~ 0.3 solar (range: 0.2–0.5)	j

[a] The X-ray luminosity of clusters (2–10 keV band). $\langle L_{\rm x}\rangle$ increases with cluster richness and with cluster type (toward compact, elliptical-rich clusters) (Bahcall 1977a,b; Sarazin 1986; Edge et al. 1991; Jones and Forman 1992; David et al. 1993; Burg et al. 1994).

[b] X-ray surface brightness distribution, $I_{\rm x}(r)$; R_c is the cluster core radius.

[c] Mean $\langle\beta\rangle$ from observations of X-ray brightness profiles (Jones and Forman 1984; Sarazin 1986).

[d] Implied spatial density profile of the hot gas in the cluster [from $I_{\rm x}(r)$; isothermal].

[e] Range of observed X-ray gas temperature in rich clusters (Edge et al. 1990; Henry and Arnaud 1991; Arnaud et al. 1992).

[f] $\beta_{\rm spect}$ is the ratio of galaxy to gas velocity dispersion: μ is mean molecular weight in amu ($\mu \simeq 0.6$), m_p is mass of the proton, σ_r is radial velocity dispersion of galaxies in the cluster, and $T_{\rm x}$ is the X-ray temperature of the gas (Lubin and Bahcall 1993).

[g] Cluster core radius determined from the X-ray distribution in the cluster (Jones and Forman 1992).

[h] Typical intracluster gas density in rich cluster cores (Jones and

3.3. The Intracluster Gas: Some Relevant Questions

Some of the fundamental questions about the intracluster gas relate to its origin, evolution, metal enrichment, hydrodynamical state in the cluster, and its relation to the distribution of galaxies and mass in the cluster. I list below some of the relevant questions and discuss a selection of these topics in the following subsections. Some of the questions posed do not yet have sufficient observational constraints to suggest a possible solution.

- What is the hydrodynamical state of the hot gas in clusters? Is it in approximate hydrostatic equilibrium with the cluster potential?
- What is the relation of the intracluster gas to the galaxies and mass in the cluster? For example (the subscripts below refer to gas, galaxies, and mass, respectively):
  - — Density profiles: $\rho_{\rm gas}(r)$ vs. $\rho_{\rm gal}(r)$ vs. $\rho_m(r)$?
  - — Temperature-velocity relation: T vs. $\sigma_{\rm gal}$ vs. σ_m?
  - — Mass: $M_{\rm gas}$ vs. $M_{\rm gal}$ vs. $M_{\rm cl}$?
  - — Profiles of the above properties:
    $T(r)$ vs. $\sigma_{\rm gal}(r)$ vs. $\sigma_m(r)$?
    $M_{\rm gas}(r)$ vs. $M_{\rm gal}(r)$ vs. $M_{\rm cl}(r)$?
  - — Core radii: R_c(gas) vs. R_c(gal) vs. $R_c(m)$?
  - — Luminosity versus galaxy-type relation: L_x vs. spiral fraction?
- What is the origin of the hot intracluster gas?
- What is the origin of the metal enrichment of the gas?
- What is the evolution of the intracluster gas?

3.4. The Intracluster Gas: Hydrostatic Equilibrium?

The standard model of clusters assumes that both the gas and the galaxies are in approximate hydrostatic equilibrium with the binding cluster potential (Bahcall and Sarazin 1977; Forman and Jones 1984; Sarazin 1986; Evrard 1990; Bahcall and Lubin 1994). In this model the gas distribution obeys

$$\frac{dP_{\rm gas}}{dr} = -\frac{GM_{\rm cl}(\leq r)\rho_{\rm gas}}{r^2} \tag{32}$$

where $P_{\rm gas}$ and $\rho_{\rm gas}$ are the gas pressure and density, and $M_{\rm cl}(\leq r)$ is the total cluster binding mass within a radius r. The cluster mass can thus be represented as

$$M_{\rm cl}(\leq r) = -\frac{kT}{\mu m_p G}\left(\frac{dln\rho_{\rm gas}(r)}{dlnr} + \frac{dlnT}{dlnr}\right) r \ , \tag{33}$$

where T is the gas temperature and μm_p is the mean particle mass of the gas.

The galaxies in the cluster respond to the same gravitational field, and they satisfy

$$M_{\rm cl}(\leq r) = -\frac{\sigma_r^2}{G}\left(\frac{dln\rho_{\rm gal}(r)}{dlnr} + \frac{dln\sigma_r^2}{dlnr} + 2A\right) r \ , \tag{34}$$

where σ_r is the radial velocity dispersion of galaxies in the cluster, $\rho_{\rm gal}(r)$ is the galaxy density profile, and A represents a possible anisotropy in the galaxy velocity distribution [$A = 1 - (\sigma_t/\sigma_r)^2$, where t and r represent the tangential and radial velocity components].

The above two relations yield

$$\beta_{\rm spec} \equiv \frac{\sigma_r^2}{kT/\mu m_p} = \frac{dln\rho_{\rm gas}(r)/dlnr + dlnT/dlnr}{dln\rho_{\rm gal}(r)/dlnr + dln\sigma_r^2/dlnr + 2A} \ , \tag{35}$$

where the $\beta_{\rm spec}$ parameter, defined by the left side of the above relation, can be determined directly from observations of cluster velocity dispersions and gas temperatures. The $\beta_{\rm spec}$ parameter represents the ratio of energy per unit mass in the galaxies to that in the gas. Observations of a large sample of clusters yield a mean best-fit value of $\beta_{\rm spec} \simeq 1 \pm 0.1$ (Lubin and Bahcall 1993; see also §3.5). This suggests that, on average, the gas and galaxies follow each other with comparable energies ($\sigma_r^2 \simeq kT/\mu m_p$). The observed mean value $\beta_{\rm spec} \simeq 1 \pm 0.1$ is consistent with the value of β determined from the right-hand side of the β relation (referred to as $\beta_{\rm fit}$, and determined from the gas and galaxy density profile fits). Using $\rho_{\rm gas}(r) \propto r^{-2}$ (§3.2) and $\rho_{\rm gal}(r) \propto r^{-2.4\pm0.2}$ (§2.6), one finds $\beta_{\rm fit} \simeq 0.85 \pm 0.1$ (for an isothermal distribution) (Bahcall and Lubin 1994). The above consistency supports the assumption that the gas is in an approximate hydrostatic equilibrium with the cluster potential, and suggests that the galaxies and gas approximately trace each other in the clusters.

3.5. The Relation between Gas and Galaxies

The hot intracluster gas in rich clusters appears to trace reasonably well the galaxies in the clusters, and—with larger uncertainty—also the cluster mass.

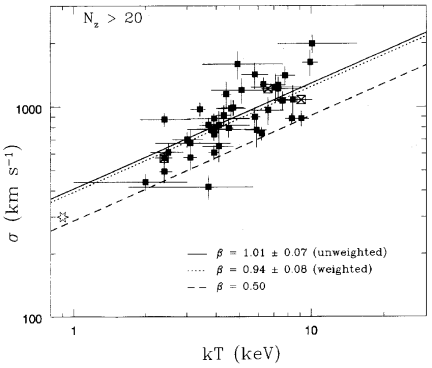

Fig. 1.— Cluster radial velocity dispersion (σ_r) vs. gas temperature (kT) for 41 clusters (Lubin and Bahcall 1993). The best-fit $\beta \equiv \sigma_r^2/(kT/\mu m_p)$ lines are shown by the solid and dotted curves, with $\beta \simeq 1$. The $\beta \simeq 0.5$ line previously proposed for a velocity bias in clusters is shown by the dashed curve; the velocity bias is inconsistent with the data.

Velocity-Temperature relation The galaxy velocity dispersion in clusters is well correlated with the temperature of the intracluster gas; it is observed (Fig. 1) that $\sigma_r^2 \simeq kT/\mu m_p$ (Lubin and Bahcall 1993). The best-fit σ–T relation is listed in §3.7. The observed correlation indicates that, on average, the energy per unit mass in the gas and in the galaxies is the same. Figure 1 shows that, unlike previous expectations, the galaxy velocities (and therefore the implied cluster mass) are not biased low with respect to the gas (and, by indirect implications, with respect to the cluster mass; see also §3.4). Results from gravitational lensing by clusters also suggest that no significant velocity bias exists in clusters, and that the gas, galaxies, and mass provide consistent tracers of the clusters. Cosmological simulations of clusters (Lubin et al. 1996) produce σ–T correlations that match well the data in Figure 1.

Density Profiles The gas density profile in clusters follows

$$\rho_{\rm gas}(r) \simeq \rho_{\rm gas}(o) \left[1 + (r/R_c)^2\right]^{-1} \ , \tag{36}$$

with core radii in the range $R_c \simeq 0.1$–$0.3h^{-1}$ Mpc (§3.2). This implies $\rho_{\rm gas}(r) \propto r^{-2}$ for $R_c < r \lesssim 1.5h^{-1}$ Mpc.

The galaxy density profile in clusters follows approximately (§2.6)

$$\rho_{\rm gal}(r) \propto r^{-2.4\pm0.2} \qquad R_c < r \lesssim 1.5h^{-1} \text{ Mpc} \tag{37}$$

with core radii $R_c \simeq 0.1 - 0.25h^{-1}$ Mpc (§2.7).

The mass density profile in clusters is less well established, but initial results from gravitational lensing distortions of background galaxies by foreground clusters suggest that the mass profile is consistent with the galaxy density profile (Tyson and Frische 1996). In the small central core regions of some clusters ($r \lesssim 100$ kpc), the mass distribution may be more compact than the gas or galaxies, with a small mass core radius of $R_c(m) \lesssim 50h^{-1}$ kpc. The results for the overall cluster, however, suggest that the distributions of gas, galaxies, and mass are similar (with the gas distribution possibly somewhat more extended than the galaxies, as seen by the mean density slopes above).

Beta-Discrepancy The mean $\beta_{\rm spec} \equiv \sigma_r^2/kT/\mu m_p \simeq 1$ result discussed above, combined with the similarity of the gas and galaxy density profile slopes (that yields $\beta_{\rm fit} \simeq 0.85 \pm 0.1$; §3.3) show that the long claimed β-discrepancy for clusters (where $B_{\rm spec} > \beta_{\rm fit}$ was claimed) has been resolved (Bahcall and Lubin 1994). The gas and galaxies trace each other both in their spatial density distribution and in their energies, as expected for a quasi-hydrostatic equilibrium.

Gas Mass Fraction The ratio of the mass of gas in clusters to the total virial cluster mass (within $\sim 1.5h^{-1}$ Mpc) is observed to be in the range

$$\frac{M_{\rm gas}}{M_{\rm cl}} \simeq 0.03{-}0.15h^{-1.5} \ , \tag{38}$$

with a median value of

$$\langle \frac{M_{\rm gas}}{M_{\rm cl}} (\lesssim 1.5h^{-1} \ {\rm Mpc}) \rangle_{\rm median} \simeq 0.07h^{-1.5} \tag{39}$$

(Jones and Forman 1992; White et al. 1993; White and Fabian 1995; Lubin et al. 1996). The implications of this result, which shows a high fraction of baryons in clusters, is discussed in §4.

The total gas mass in clusters, $\sim 10^{13}$–$10^{14}h^{-2.5}M_{\odot}$, is generally larger than the total mass of the luminous parts of the galaxies (especially for low values of h). With so much gas mass, it is most likely that a large fraction of the intracluster gas is of cosmological origin (rather than all the cluster gas being stripped out of galaxies). Additional optical-X-ray correlations of clusters are summarized in §3.7.

3.6. Metal Abundance in Intracluster Gas

The iron abundance in the intracluster gas is observed to be ~ 0.3 solar, with only small variations ($\pm \sim 0.1$) from cluster to cluster (e.g., Jones and Forman 1992). A strong correlation between the total iron mass in clusters and the total luminosity of the E + SO cluster galaxies is observed (Jones and Forman 1992). The metal enrichment of the intracluster gas is likely caused by gas stripped out of the elliptical galaxy members.

The iron abundance profile as a function of radius from the cluster center is generally flat, i.e., a constant abundance at all radii (except for some poor, low-mass clusters dominated by a single massive galaxy).

No evolution is observed in the overall iron abundance of clusters to $z \sim 0.4$ (Mushotzky 1996).

Recent results using ASCA observations (Mushotzky 1996) of different element abundances in nearby clusters (O, Ne, Mg, Si, S, Ar, Ca) suggest a SNII origin for the metals (resulting from early massive stars) rather than the expected SNIa. These new results will be expanded in the near future as additional accurate X-ray data become available and will provide further clues regarding the origin of the metallicity of the intracluster gas.

3.7. X-Ray–Optical Correlations of Cluster Properties

Some observed correlations between X-ray and optical properties are listed in Table 7 (Bahcall 1977a,b; Edge and Stewart 1991; David et al. 1993; Lubin and Bahcall 1993).

3.8. The X-Ray Luminosity Function of Clusters

The X-ray luminosity function of clusters (the number density of clusters with X-ray luminosity $L_{\rm x}$ to $L_{\rm x} + dL_{\rm x}$) is approximately (Edge et al. 1990)

$$\Phi_{\rm x}(L_{\rm x})dL_{\rm x} \simeq 2.7 \times 10^{-7}(L_{\rm x}/10^{44})^{-1.65}\exp(-L_{\rm x}/8.1 \times 10^{44})(dL_x/10^{44})\ {\rm Mpc}^{-3} \qquad (40)$$

for $h = 0.5$, where $L_{\rm x}$ is the 2–10-keV X-ray luminosity in units of $\rm erg\,s^{-1}$ (for $h = 0.5$). The luminosity function can also be approximated as a power law (Edge et al. 1990)

$$\Phi_{\rm x}(L_{\rm x})dL_{\rm x} \simeq 2.2 \times 10^{-7}(L_{\rm x}/10^{44})^{-2.17}(dL_{\rm x}/10^{44})\ {\rm Mpc}^{-3}\ (h = 0.5). \qquad (41)$$

The number of X-ray clusters with X-ray luminosity brighter than $L_{\rm x}$ is approximately

$$n_c(> L_{\rm x}) \simeq 2 \times 10^{-7}(L_{\rm x}/10^{44})^{-1.17}\ {\rm Mpc}^{-3}\ (h = 0.5). \qquad (42)$$

The observed evolution of the X-ray cluster luminosity function suggests fewer high-luminosity clusters in the past ($z \gtrsim 0.5$) (Edge et al. 1990, Henry et al. 1992). Additional data is required, however, to confirm and better assess the cluster evolution.

3.9. Cooling Flows in Clusters

Cooling flows are common at the dense cores of rich clusters; X-ray images and spectra of $\sim 50\%$ of clusters suggest that the gas is cooling rapidly at their centers (Sarazin 1986; Fabian 1992). Typical inferred cooling rates are $\sim 100\mathcal{M}_\odot/{\rm yr}$. The gas cools within $r \lesssim 100h^{-1}$ kpc of the cluster center (generally centered on the brightest galaxy). The cooling flows often show evidence for optical line emission, blue stars, and in some cases evidence for colder material in HI or CO emission, or X-ray absorption.

3.10. The Sunyaev-Zeldovich Effect in Clusters

The Sunyaev–Zeldovich (1972) effect is a perturbation to the spectrum of the cosmic microwave background radiation as it passes through the hot dense intracluster gas. It is caused by inverse Compton scattering of the radiation by the electrons in the cluster gas.

Table 7: Correlations Between X-Ray and Optical Properties.[a]

Properties	Correlation
σ_r-T	σ_r (km s^{-1}) $\simeq (332 \pm 52)[kT$ (kev)$]^{0.6\pm0.1}$
T-$N_{0.5}$	kT (keV)$\simeq 0.3 N_{0.5}^{0.95\pm0.18}$
$L_{\rm x}$-$N_{0.5}$	$L_{\rm x}$(bol)$\sim 1.4 \times 10^{40} N_{0.5}^{3.16\pm0.15} h^{-2}$
L_x-$f_{\rm sp}$	$L_{\rm x}$(bol)$\simeq 0.6 \times 10^{43} f_{\rm sp}^{-2.16\pm0.11} h^{-2}$
$f_{\rm sp}$-T	$f_{\rm sp} \simeq 1.2[kT$ (kev)$]^{-0.94\pm0.38}$
T-$L_{\rm x}$	kT (keV)$\simeq 0.3[L_{\rm x}$(bol)$h^2/10^{40}]^{0.297\pm0.004}$

[a] σ_r is the galaxy line-of-sight velocity dispersion in the cluster (km s^{-1}). T is the temperature of the intracluster gas [kT (keV)]. $N_{0.5}$ is the central galaxy density in the cluster [number of galaxies brighter than $m_3 + 2^m$, within $r \leq 0.5 h_{50}^{-1} = 0.25 h^{-1}$ of the cluster center (Bahcall 1977a; Edge and Stewart 1991)]. $L_{\rm x}$(bol) is the bolometric X-ray luminosity of the cluster (erg s^{-1}). $f_{\rm sp}$ is the fraction of spiral galaxies in the cluster ($\lesssim 1.5 h^{-1}$ Mpc) (Bahcall 1977b; Edge and Stewart 1991). Typical uncertainties of the coefficients are $\sim 50\%$ (see references).

At the long-wavelength side of the background radiation spectrum, the hot gas lowers the brightness temperature seen through the cluster center by the fractional decrement

$$\frac{\delta T}{T} = -2\tau_0 \frac{kT_{\rm x}}{m_e c^2}, \tag{43}$$

where $T = 2.73$ K is the microwave radiation temperature, τ_0 is the Thomson scattering optical depth through the cluster ($\tau_0 = \sigma_T \int n_e dl$, where σ_T is the Thomson scattering cross section and dl is the distance along the line of sight), $T_{\rm x}$ is the intracluster gas temperature, and m_e is the electron mass.

For typical observed rich cluster parameters of $L_{\rm x} \sim 10^{44} h^{-2}$ erg s^{-1}, $R_c \sim 0.2 h^{-1}$ Mpc, and $kT_{\rm x} \simeq 4$ keV, the bremsstrahlung relation ($L_{\rm x} \propto n_e^2 R_c^3 T_{\rm x}^{0.5}$, §3.1) implies a central gas density of $n_e \simeq 3 \times 10^{-3} h^{1/2}$ electrons cm^{-3}, thus yielding $\tau_0 \simeq 3 \times 10^{-3} h^{-1/2}$ [$\tau_0 = 0.0064 n_e({\rm cm}^{-3}) R_c({\rm kpc})$]. Therefore

$$\frac{\delta T}{T} \sim -6 \times 10^{-5} h^{-1/2}. \tag{44}$$

This temperature decrement remains constant over the cluster core diameter

$$\theta_c \simeq \frac{2 H_0 R_c}{cz} \simeq \frac{0.5}{z} \text{ arcmin} \tag{45}$$

and decreases at larger separations.

The effect has been detected in observations of some rich, X-ray luminous clusters (e.g., Coma, A665, A2163, A2218, Cl 0016+16) (Birkinshaw et al. 1984; Jones et al. 1993; Wilbanks et al. 1994; Herbig et al. 1995).

4. The Baryon Fraction in Clusters

Rich clusters of galaxies provide the best laboratory for studying the baryon fraction (i.e., the ratio of the mass in baryons to the total mass of the system) on relatively large scales of $\sim$ Mpc. The mass of baryons in clusters is composed of *at least* two components: the hot intracluster gas (§3) and the luminous parts of the galaxies.

The baryon fraction in clusters is therefore

$$\frac{\Omega_b}{\Omega_m} \gtrsim \frac{M_{\rm gas} + M_{\rm stars}}{M_{\rm cl}} \simeq 0.07 h^{-1.5} + 0.05 \ , \tag{46}$$

where the first term on the right-hand side represents the gas mass ratio (§3.5) and the second term corresponds to the stellar (luminous) contribution.

The baryon density required by big-bang nucleosynthesis is (Walker et al. 1991)

$$\Omega_b(\mathrm{BBN}) \simeq 0.015h^{-2} \ . \tag{47}$$

Comparison of the above relations indicates that if $\Omega_m = 1$ then there are many more baryons observed in clusters than allowed by nucleosynthesis. In fact, combining the two relations yields an Ω_m value for the mass-density of

$$\Omega_m \lesssim \frac{\Omega_b}{0.07h^{-1.5} + 0.05} \simeq \frac{0.015h^{-2}}{0.07h^{-1.5} + 0.05} \sim 0.2 \tag{48}$$

for the observed range of $h \sim 0.5{-}0.8$. Therefore, the baryon density given by nucleosynthesis and the high baryon content observed in clusters (mainly in the hot intracluster gas) suggest that $\Omega_m \simeq 0.2$. This assumes, as expected on this large scale (and as seen in simulations), that the baryons are not segregated relative to the dark matter in clusters (White et al. 1993).

Figure 2 compares the observed gas mass fraction in clusters ($\propto$ baryon fraction) with expectations from cosmological simulations of $\Omega_m = 1$ and $\Omega_m = 0.45$ cold-dark-matter (CDM) flat models (Lubin et al. 1996). The results show, as expected, that the $\Omega_m = 1$ model predicts a much lower gas mass fraction than observed, by a factor of ~ 3. A low-density CDM model with $\Omega_m \sim 0.2{-}0.3$ (in mass) best matches the data, as expected from the general analysis discussed above (see White et al. 1993; White and Fabian 1995; Lubin et al. 1996).

In summary, the high baryon fraction observed in clusters suggests, independent of any specific model, that the mass density of the universe is low, $\Omega_m \sim 0.2{-}0.3$. This provides a powerful constraint on high-density ($\Omega_m = 1$) models; if $\Omega_m = 1$, a resolution of this baryon problem needs to be found.

5. Cluster Masses

The masses of clusters of galaxies within a given radius, $M(\leq r)$, can be determined from three independent methods:

a) Optical: galaxy velocity dispersion (and distribution) assuming hydrostatic equilibrium (§3.3);

b) X-Rays: hot gas temperature (and distribution) assuming hydrostatic equilibrium (§3.3);

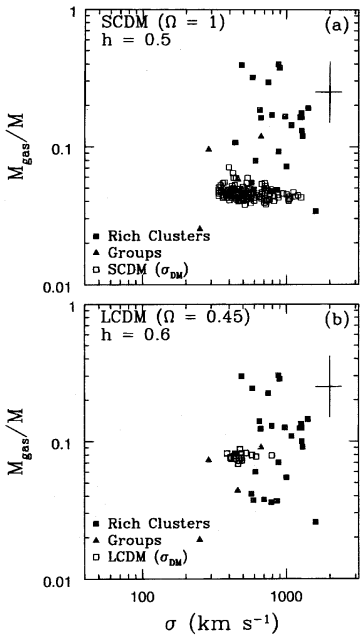

Fig. 2.— Observed and simulated gas mass fraction ($M_{\rm gas}/M$) vs. line-of-sight velocity dispersion for rich clusters (Lubin et al. 1996). A typical 1σ uncertainty is shown. The simulated results (open squares) present the dark matter velocity dispersion; the galaxy velocity dispersion is lower by $b_v \sim 0.8$ for SCDM and by $b_v \sim 0.9$ for LCDM. (a) SCDM ($\Omega_m = 1, h = 0.5$); (b) LCDM ($\Omega_m = 0.45, h = 0.6$).

c) Lensing: gravitational distortions of background galaxies (Tyson et al. 1990, 1996; Kaiser and Squires 1993). This method determines directly the surface mass overdensity.

The first two methods were discussed in §§2 and 3; the last (and newest) method is discussed in this book by Narayan. (See also Tyson et al. 1990, 1996; Kaiser and Squires 1993; Smail et al. 1995, and references therein).

The galaxy and hot gas methods yield cluster masses that are consistent with each other as discussed in §3 (with $\sigma_r^2 \simeq kT/\mu m_p$). Gravitational lensing results, which provide direct information about cluster masses, are available only for a small number of clusters so far (with data rapidly increasing). For all but one of the clusters the masses determined from lensing are consistent, within the uncertainties, with the masses determined from the galaxies and hot gas methods (see Bahcall 1995 for a summary). Some differences in masses between the different methods are expected for individual clusters due to anisotropic velocities, cluster orientation (yielding larger lensing surface mass densities for clusters elongated in the line-of-sight, and vice versa), and sub-structure in clusters. On average, however, all three independent methods yield cluster masses that are consistent with each other. This triple check on cluster masses provides strong support for the important cluster mass determinations.

The masses of rich clusters range from $\sim 10^{14}$ to $\sim 10^{15} h^{-1}\ M_\odot$ within $1.5h^{-1}$ Mpc radius of the cluster center. When normalized by the cluster luminosity, a robust mass-to-light ratio is determined for nearby clusters, with only small variations from cluster to cluster (§2.10)

$$\frac{M}{L_B}(\text{clusters}) \simeq 300 \pm 100h \frac{M_\odot}{L_\odot}\ . \tag{49}$$

This result is similar to the one obtained from the baryon fraction in §4.

If, as desired by theoretical arguments, the universe has critical mass density $\Omega_m = 1$, than most of the mass in the universe *cannot* be associated with galaxies, groups, and clusters; the mass distribution in this case would be strongly biased (i.e., mass does not follow light, with the mass distributed considerably more diffusely than the light).

6. Where is the Dark Matter?

A recent analysis of the mass-to-light ratio of galaxies, groups and clusters by Bahcall, Lubin and Dorman (1995) suggests that while the M/L ratio of galaxies increases with scale up to radii of $R \sim 0.1$–$0.2h^{-1}$ Mpc, due to the large dark halos around galaxies (see Fig. 3; also Ostriker et al. 1974), this ratio appears to flatten and remain approximately

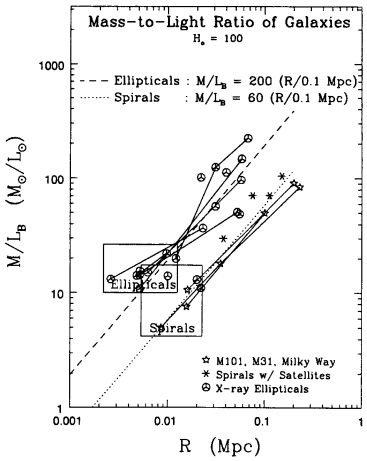

Fig. 3.— Mass-to-light ratio of spiral and elliptical galaxies as a function of scale (Bahcall, Lubin and Dorman 1995). The large boxes indicate the typical ($\sim 1\sigma$) range of M/L_B for bright ellipticals and spirals at their luminous (Holmberg) radii. (L_B refers to *total* corrected blue luminosity; see text.) The best-fit $M/L_B \propto R$ lines are shown.

constant for groups and rich clusters, to scales of ~ 1.5 Mpc, and possibly even to the larger scales of superclusters (Fig. 4). The flattening occurs at $M/L_B \simeq 200$–$300h$, corresponding to $\Omega_m \sim 0.2$. This observation suggests that most of the dark matter is associated with the dark halos of galaxies. Unlike previous expectations, this result implies that clusters do *not* contain a substantial amount of *additional* dark matter, other than that associated with (or torn-off from) the galaxy halos, and the hot intracluster medium. Bahcall et al. (1995) suggest that the relatively large M/L_B ratio of clusters ($\sim 300h$) results mainly from a high M/L_B ration of elliptical/SO galaxies. They show (Fig. 3) that ellipticals have an M/L_B ratio that is approximately 3 to 4 times larger than typical spirals at the same radius [$(M/L_B)_s \sim 100h$ and $(M/L_B)_e \sim 400h$ within $r \lesssim 200h^{-1}$ Kpc]. Since clusters are dominated by elliptical and SO galaxies, a high M/L_B ratio results.

Unless the distribution of matter is very different from the distribution of light, with large amounts of dark matter in the "voids" or on very large scales, the above results suggest that the mass density in the universe may be low, $\Omega_m \sim 0.2$ (or $\Omega_m \sim 0.3$ for a small bias of $b \sim 1.5$, where the bias factor b relates the overdensity in galaxies to the overdensity in mass: $b \equiv (\Delta\rho/\rho)_{\rm gal}/(\Delta\rho/\rho)_m$).

7. The Mass Function of Clusters

The observed mass function (MF), $n(>M)$, of clusters of galaxies, which describes the number density of clusters above a threshold mass M, can be used as a critical test of theories of structure formation in the universe. The richest, most massive clusters are thought to form from rare high peaks in the initial mass-density fluctuations; poorer clusters and groups form from smaller, more common fluctuations. Bahcall and Cen (1993) determined the MF of clusters of galaxies using both optical and X-ray observations of clusters. Their MF is presented in Figure 5. The function is well fit by the analytic expression

$$n(>M) = 4 \times 10^{-5} (M/M^*)^{-1} \exp(-M/M^*) h^3 \ {\rm Mpc}^{-3} \ , \tag{50}$$

with $M^* = (1.8 \pm 0.3) \times 10^{14} h^{-1} \ M_\odot$, (where the mass M represents the cluster mass within $1.5h^{-1}$ Mpc radius).

The observed cluster mass function is compared in Figure 5 with expectations from different cold-dark-matter cosmologies using large-scale simulations (Bahcall and Cen 1992). The comparison shows that the cluster MF is indeed a powerful discriminant among models. The standard CDM model ($\Omega_m = 1$) cannot reproduce the observed MF for any bias parameter; when normalized to the COBE microwave background fluctuations on large scales, this model produces too many massive clusters, unseen by the observations. A low-density CDM

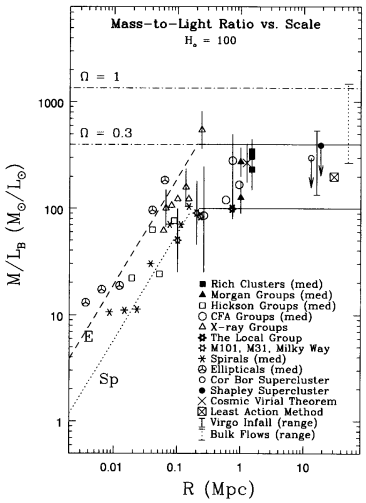

Fig. 4.— Composite mass-to-light ratio of different systems—galaxies, groups, clusters, and superclusters—as a function of scale (Bahcall et al. 1995). The best-fit $M/L_B \propto R$ lines for spirals and ellipticals (from Fig. 3) are shown. We present median values at different scales for the large samples of galaxies, groups and clusters, as well as specific values for some individual galaxies, X-ray groups, and superclusters. Typical 1σ uncertainties and 1σ scatter around median values are shown. Also presented, for comparison, are the M/L_B (or equivalently Ω) determinations from the cosmic virial theorem, the least action method, and the *range* of various reported results from the Virgocentric infall and large-scale bulk flows (assuming mass traces light). The M/L_B expected for $\Omega = 1$ and $\Omega = 0.3$ are indicated.

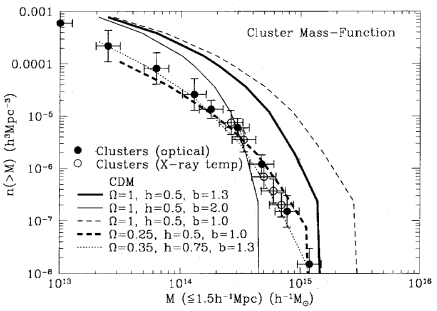

Fig. 5.— Cluster mass functions from observations and from CDM dimulations (Bahcall and Cen 1992).

model on the other hand, with $\Omega_m \sim 0.2-0.3$ (with or without a cosmological constant), appears to fit well the observed cluster MF (Fig. 5).

8. Quasar-Cluster Association

Imaging and spectroscopic data (Yee et al. 1987; Ellingson et al. 1991; Yee et al. 1992) indicate that quasars are found in environments significantly richer than those of average galaxies. The data show a positive association of quasars with neighboring galaxies.

Optically selected quasars to $z \lesssim 0.7$ exhibit a quasar–galaxy cross-correlation function amplitude, A_{qg}, that is approximately 2.3 times stronger than the galaxy-galaxy correlation amplitude (to separations $r \lesssim 0.25h^{-1}$ Mpc):

$$\langle A_{qg} \rangle \simeq 2.3 \langle A_{gg} \rangle \simeq 46. \tag{51}$$

This excess correlation suggests that the quasars are typically located in groups of galaxies with a *mean* richness

$$\langle N_R \rangle = n_g \int_0^{1.5} A_{qg} r^{-1.8} 4\pi r^2 dr \simeq 12 \text{ galaxies} \tag{52}$$

(where $n_g \simeq 0.015$ Mpc^{-3} is the mean density of galaxies). The range of individual group richnesses is, however, wide.

Radio-loud quasars at $z \lesssim 0.5$ are found in similar environments to those of the optical quasars above. At $0.5 \lesssim z \lesssim 0.7$, the radio quasars appear to be located in richer environments, with

$$\langle A_{qg} \rangle \simeq 8 \langle A_{gg} \rangle \simeq 160 \qquad (\text{radio quasars, } 0.5 \lesssim z \lesssim 0.7). \tag{53}$$

This cross-correlation amplitude corresponds to a *mean* environment of rich clusters ($R \sim 0$, $N_R \sim 40$). Radio quasars at these redshifts are thus typically found in rich clusters.

The average galaxy velocity dispersion of the parent clusters associated with the quasars (Ellingson et al. 1991; Yee et al. 1992) is

$$\sigma_r \sim 500 \text{ km s}^{-1}. \tag{54}$$

The observed auto-correlation function of optically selected quasars is approximately (Shaver 1988)

$$\xi_{qq}(r, z \sim 0) \simeq 10^{2 \pm 0.2} [r(\text{Mpc})]^{-1.8} \tag{55}$$

The quasar correlation strength is intermediate between the correlation of individual galaxies and the correlation of rich clusters. This correlation strength is consistent with the quasars location in groups of the above mean richness, as would be suggested by the richness-dependent cluster correlation function (§10). The quasars may thus trace the correlation function of their parent clusters (Bahcall and Chokshi 1991).

Similar results are observed for the association of radio galaxies with groups and clusters. This association explains the observed increase in the strength of the radio galaxy correlation function over the general galaxy correlations (Bahcall and Chokshi 1992).

9. Superclusters

Rich clusters of galaxies are powerful tracers of the large-scale structure of the universe (Bahcall 1988, Peebles 1993). I summarize in the sections below the use of clusters in tracing the large-scale structure; I include superclusters (§9), statistics of the cluster correlation function (§10), and peculiar motions on large scales (§11).

9.1. Supercluster Properties

Redshift surveys of galaxies reveal that superclusters are very large, high-density systems of galaxies that are flattened or filamentary in shape, extending to tens of Mpc. The superclusters appear to surround large under-dense regions ("voids") of comparable sizes creating a "cellular-like" morphology of the universe on large scales (Gregory and Thompson 1978; Gregory et al. 1981; Chincarini et al. 1981; Giovanelli et al. 1986; de-Lapparent et al. 1986; da Costa et al. 1988; Rood 1988; Schectman et al. 1996; Landy et al. 1996).

Large scale superclusters have been identified very effectively by rich clusters of galaxies (Bahcall and Soneira 1984), like high mountain peaks tracing mountain chains. Superclusters are generally defined as clusters of rich clusters of galaxies above a given spatial density enhancement f. Here $f \equiv n_c(SC)/n_c$, where $n_c(SC)$ is the number density of clusters in a supercluster and n_c is the mean number density of clusters. The observed superclusters are large flattened systems, extending to $\sim 150h^{-1}$ Mpc in size. The superclusters typically contain several clusters. The high-density superclusters generally surround low-density regions.

A complete catalog of superclusters was constructed by Bahcall and Soneira (1984) to $z \lesssim 0.08$. The catalog identifies all superclusters that have a spatial density enhancement $f \geq 20$. The mean number density of the Bahcall-Soneira superclusters is $\sim 10^{-6}h^3$ Mpc^{-3},

Table 8: Global Properties of Bahcall–Soneira Superclusters.

Property	$f = 20$ superclusters
Number density of SCs	$\sim 10^{-6} h^3\,\mathrm{Mpc}^{-3}$
Number of clusters per SC	2–15 clusters
Fraction of clusters in SCs	54%
Size of largest SC	$\sim 150 h^{-1}\,\mathrm{Mpc}$
SC shape	Flattened
Volume of space occupied by SCs	$\sim 3\%$

with a mean separation between superclusters of $\sim 100 h^{-1}$ Mpc. A summary of the main properties of the superclusters is presented in Table 8.

The superclusters trace well the structure observed in the more detailed, but smaller, galaxy redshift surveys.

9.2. Superclusters and Pencil-Beam Surveys

Observations of the redshift distribution of galaxies in narrow (~ 40 arcmin) pencil-beam surveys to $z \lesssim 0.3$ (Broadhurst et al. 1990; hereafter BEKS) reveal a highly clumped and apparently periodic distribution of galaxies. The distribution features peaks of galaxy counts with an apparently regular separation of 128 Mpc, with few galaxies between the peaks. What is the origin of this clumpy, periodic distribution of galaxies? What does it imply for the nature of the large-scale structure and the properties discussed above? Bahcall (1991) investigated these questions observationally, by comparing the specific galaxy distribution with the distribution of known superclusters.

Bahcall showed that the observed galaxy clumps originate from the tails of large superclusters (§9.1). When the narrow-beams intersect these superclusters, which have a mean separation of ~ 100 Mpc, the BEKS galaxy distribution is reproduced.

The redshift distribution of the superclusters is essentially identical to the galaxy redshift distribution, i.e., it reproduces the observed peaks in the BEKS survey, for $z \lesssim 0.1$. This indicates that the galaxy clumps observed in the pencil-beam survey originate from these superclusters as the beam crosses the superclusters' surface. The main superclusters that

contribute to the clumps were identified. For example, the first northern clump originates from the Coma-Hercules supercluster (= the Great-Wall); the second northern clump is mostly due to the large Corona Borealis supercluster.

The narrow-beam survey of BEKS is directed toward the north and south galactic poles. Some of the Bahcall-Soneira superclusters coincident with the BEKS peaks are located at projected distances of up to $\sim$ 50–100 Mpc from the poles. This suggests that the high-density supercluster regions are embedded in still larger halo surfaces, $\sim$ 100 Mpc in size, and that these large structures surround large underdense regions. The observed number of clumps and their mean separation are consistent with the number density of superclusters and their average extent (§9.1).

The narrow widths of the BEKS peaks are consistent with, and imply, flat superclusters. From simulations of superclusters and pencil-beams, Bahcall, Miller, and Udomprasert (1996) find that the observed peak-widths distribution is consistent with that expected of randomly placed superclusters with $\lesssim$ 15 Mpc width and $\sim$ 150 Mpc extent.

The Bahcall-Soneira superclusters may exhibit weak positive correlations on scales $\sim$ 100–150 Mpc (Bahcall and Burgett 1986). This implies that the superclusters, and thus their related galaxy clumps, are not randomly distributed but are located in some weakly correlated network of superclusters and voids, with typical mean separation of $\sim$ 100 Mpc. This picture is consistent with statistical analyses of the BEKS distribution as well as with the observational data of large-scale structure. The apparent periodicity in the galaxy distribution suggested by BEKS is expected to be greatly reduced when pencil-beams in various directions are combined; the scale reflects the typical *mean* separation between large superclusters, ~ 100–$150h^{-1}$ Mpc, but with large variations at different locations.

10. The Cluster Correlation Function

The correlation function of clusters of galaxies efficiently quantifies the large-scale structure of the universe. Clusters are correlated in space more strongly than are individual galaxies, by an order of magnitude, and their correlation extends to considerably larger scales ($\sim 50h^{-1}$ Mpc). The cluster correlation strength increases with richness ($\propto$ luminosity or mass) of the system from single galaxies to the richest clusters (Bahcall and Soneira 1983; Bahcall and West 1992). The correlation strength also increases with the mean spatial separation of the clusters (Szalay and Schramm 1985; Bahcall and Burgett 1986; Bahcall and West 1992). This dependence results in a "universal" dimensionless cluster correlation function; the cluster dimensionless correlation scale is constant for all clusters when normalized

by the mean cluster separation.

Empirically, two general relations have been found (Bahcall and West 1992) for the correlation function of clusters of galaxies, $\xi_i = A_i r^{-1.8}$:

$$A_i \propto N_i \ , \tag{56}$$

$$A_i \simeq (0.4 d_i)^{1.8} \ , \tag{57}$$

where A_i is the amplitude of the cluster correlation function, N_i is the richness of the galaxy clusters of type i (§2.2), and d_i is the mean separation of the clusters. Here $d_i = n_i^{-1/3}$, where n_i is the mean spatial number density of clusters of richness N_i (§2.3) in a volume-limited, richness-limited complete sample. The first relation, Eq. (56), states that the amplitude of the cluster correlation function increases with cluster richness, i.e., rich clusters are more strongly correlated than poorer clusters. The second relation, Eq. (57), states that the amplitude of the cluster correlation function depends on the mean separation of clusters (or, equivalently, on their number density); the rarer, large mean separation richer clusters are more strongly correlated than the more numerous poorer clusters. Eqs. (56) and (57) relate to each other through the richness function of clusters, i.e., the number density of clusters as a function of their richness. Equation (57) describes a universal scale-invariant (dimensionless) correlation function with a correlation scale $r_{o,i} = A_i^{1/1.8} \simeq 0.4 d_i$ (for $30 \lesssim d_i \lesssim 90 h^{-1}$ Mpc).

There are some conflicting statements in the literature about the precise values of the correlation amplitude, A_i. Nearly all these contradictions are caused by not taking account of Eq. (56). When apples are compared to oranges, or the clustering of rich clusters is compared to the clustering of poorer clusters, differences are expected and observed.

Figure 6 clarifies the observational situation. The $A_i(d_i)$ relation for groups and clusters of various richnesses is presented in the figure. The recent automated cluster surveys of APM (Dalton et al. 1992) and EDCC (Nichol et al. 1992) are consistent with the predictions of Eqs. (56) and (57), as is the correlation function of X-ray selected ROSAT clusters of galaxies (Romer et al. 1994). Bahcall and Cen (1994) show that a flux-limited sample of X-ray selected clusters will exhibit a correlation scale that is smaller than that of a volume-limited, richness-limited sample of comparable apparent spatial density since the flux-limited sample contains poor groups nearby and only the richest clusters farther away. Using the richness-dependent cluster correlations of Eqs. (56) and (57), Bahcall and Cen (1994) find excellent agreement with the observed flux-limited X-ray cluster correlations of Romer et al. (1994).

The strong correlation amplitude of galaxy clusters, and the large scales to which clusters are observed to be positively correlated ($\sim 50{-}100 h^{-1}$ Mpc), complement and quantify the superclustering of galaxy clusters discussed in §9. Clusters of galaxies are strongly clustered

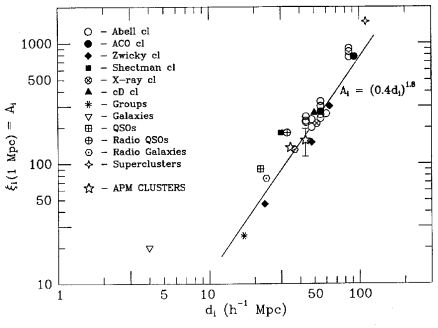

Fig. 6.— The *universal* dimensionless cluster correlations: the dependence of correlation amplitude on mean separation (Bahcall and West 1992). Data points include different samples and catalogs of clusters and groups, as well as X-ray-selected and cD clusters. Quasars and radio galaxies, as represented by their parent groups, are also included. The APM results are presented; they are consistent with the expected relation.

in superclusters of large scales (§9), consistent with the strong cluster correlations to these scales (§10).

This fundamental observed property of clusters of galaxies—the cluster correlation function—can be used to place strong constraints on cosmological models and the density parameter Ω_m by comparison with model expectations. Bahcall and Cen (1992) contrasted these cluster observations with standard and nonstandard CDM models using large N-body simulations ($400h^{-1}$ box, $10^{7.2}$ particles). They find that none of the standard $\Omega_m = 1$ CDM models can fit consistently the strong cluster correlations. A low-density ($\Omega_m \sim 0.2{-}0.3$) CDM-type model (with or without a cosmological constant), however, provides a good fit to the cluster correlations (see Figs. 7–9) as well as to the observed cluster mass-function (§7, Fig. 5). This is the first CDM-type model that is consistent with the high amplitude and large extent of the correlation function of the Abell, APM, and EDCC clusters. Such low-density models are also consistent with other observables as discussed in this paper. The Ω_m constraints of these cluster results are model dependent; a mixed hot + cold dark matter model, for example, with $\Omega_m = 1$, is also consistent with these cluster data (see Primack's chapter in this book).

The CDM results for clusters corresponding to the rich Abell clusters (richness class $R \geq 1$) with $d = 55h^{-1}$ Mpc are presented in Figure 7 together with the observed correlations (Bahcall and Soneira 1983; Peacock and West 1992). The results indicate that the standard $\Omega_m = 1$ CDM models are inconsistent with the observations; they cannot provide either the strong amplitude or the large scales ($\gtrsim 50h^{-1}$ Mpc) to which the cluster correlations are observed. Similar results are found for the APM and EDCC clusters.

The low-density, low-bias model is consistent with the data; it reproduces both the strong amplitude and the large scale to which the cluster correlations are detected.

The dependence of the observed cluster correlation on d was also tested in the simulations. The results are shown in Figure 8 for the low-density model. The dependence of correlation amplitude on mean separation is clearly seen in the simulations. To compare this result directly with observations, I plot in Figure 9 the dependence of the correlation scale, r_o, on d for both the simulations and the observations. The low-density model agrees well with the observations, yielding $r_o \approx 0.4d$, as observed. The $\Omega_m = 1$ model, while also showing an increase of r_o with d, yields considerably smaller correlation scales and a much slower increase of $r_o(d)$.

What causes the observed dependence on cluster richness [Eqs. (56–57]? The dependence, seen both in the observations and in the simulations, is most likely caused by the statistics of rare peak events, which Kaiser (1984) suggested as an explanation of the ob-

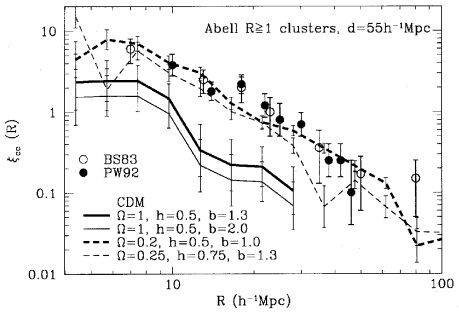

Fig. 7.— Two-point correlation function of Abell $R \geq 1$ clusters, with mean separation $55h^{-1}$ Mpc, from observations and the CDM simulations (Bahcall and Cen 1992).

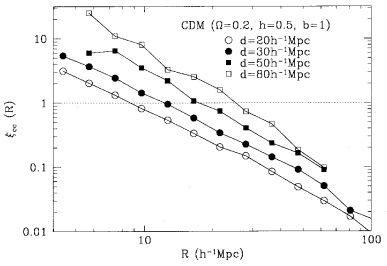

Fig. 8.— Model dependence of the cluster correlation function on mean separation d (CDM simulation: $\Omega = 0.2, h = 0.5, b = 1$) (from Bahcall and Cen 1992).

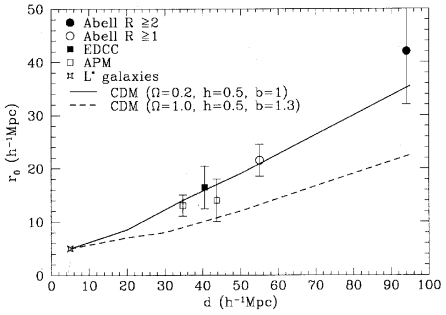

Fig. 9.— Correlation length as a function of cluster separation, from both observations and simulations (Bahcall and Cen 1992).

served strong increase of correlation amplitude from galaxies to rich clusters. The correlation function of rare peaks in a Gaussian field increases with their selection threshold. Since more massive clusters correspond to a higher threshold, implying rarer events and thus larger mean separation, Eq. (57) results. A fractal distribution of galaxies and clusters would also produce Eq. (57) (e.g., Szalay and Schramm 1985).

11. Peculiar Motions of Clusters

How is the mass distributed in the universe? Does it follow, on the average, the light distribution? To address this important question, peculiar motions on large scales are studied in order to directly trace the mass distribution. It is believed that the peculiar motions (motions relative to a pure Hubble expansion) are caused by the growth of cosmic structures due to gravity. A comparison of the mass-density distribution, as reconstructed from peculiar velocity data, with the light distribution (i.e., galaxies) provides information on how well the mass traces light (see chapter by Dekel, and 1994). The basic underlying relation between peculiar velocity and density is given by

$$\vec{\nabla} \cdot \vec{v} = -\Omega_m^{0.6} \delta_m = -\Omega_m^{0.6} \delta_g / b \tag{58}$$

where $\delta_m \equiv (\Delta\rho/\rho)_m$ is the mass overdensity, δ_g is the galaxy overdensity, and $b \equiv \delta_g/\delta_m$ is the bias parameter discussed in §6. A formal analysis yields a measure of the parameter $\beta \equiv \Omega_m^{0.6}/b$. Other methods that place constraints on β include the anisotropy in the galaxy distribution in the redshift direction due to peculiar motions (see Strauss and Willick 1995 for a review).

Measuring peculiar motions is difficult. The motions are usually inferred with the aid of measured distances to galaxies or clusters that are obtained using some (moderately-reliable) distance-indicators (such as the Tully-Fisher or $D_n - \sigma$ relations), and the measured galaxy redshift. The peculiar velocity v_p is then determined from the difference between the measured redshift velocity, cz, and the measured Hubble velocity, v_H, of the system (the latter obtained from the distance-indicator): $v_p = cz - v_H$.

A summary of all measurements of β made so far is presented in Strauss and Willick (1995). The dispersion in the current measurements of β is very large; the various determinations range from $\beta \sim 0.4$ to ~ 1, implying, for $b \simeq 1, \Omega_m \sim 0.2$ to ~ 1. No strong conclusion can therefore be reached at present regarding the values of β or Ω_m. The larger and more accurate surveys currently underway, including high precision velocity measurements, will likely lead to the determination of β and possibly its decomposition into Ω_m and b (e.g., Cole et al. 1994).

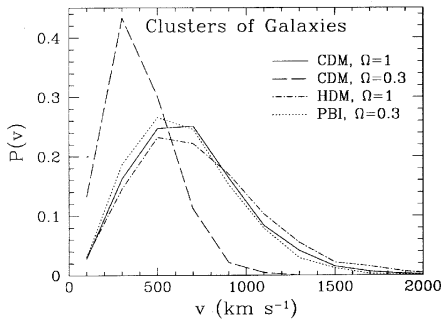

Fig. 10.— Differential three-dimensional peculiar velocity distribution of rich clusters of galaxies for four cosmological models (Bahcall, Gramann and Cen 1994).

Clusters of galaxies can also serve as efficient tracers of the large-scale peculiar velocity field in the universe (Bahcall, Gramann and Cen 1994). Measurements of cluster peculiar velocities are likely to be more accurate than measurements of individual galaxies, since cluster distances can be determined by averaging a large number of cluster members as well as by using different distance indicators. Using large-scale cosmological simulations, Bahcall et al. (1994) find that clusters move reasonably fast in all the cosmological models studied, tracing well the underlying matter velocity field on large scales. The clusters exhibit a Maxwellian distribution of peculiar velocities as expected from Gaussian initial density fluctuations. The model cluster 3-D velocity distribution, presented in Figure 10, typically peaks at $v \sim 600$ km s^{-1} and extends to high cluster velocities of ~ 2000 km s^{-1}. The low-density CDM model exhibits lower velocities (Fig. 10). Approximately 10% of all model rich clusters (1% for low-density CDM) move with $v \gtrsim 10^3$ km s^{-1}. A comparison of model expectation with recent, well calibrated cluster velocity data (Giovanelli et al. 1996) is presented in Figure 11 (Bahcall and Oh 1996). The comparison between models and observations suggests that the cluster velocity data is consistent with a low-density CDM model, and is inconsistent with a standard $\Omega_m = 1$ CDM model, since no high velocity clusters are observed.

Cen, Bahcall and Gramann (1994) determined the expected velocity correlation function of clusters in different cosmologies. They find that close cluster pairs, with separations $r \lesssim 10h^{-1}$ Mpc, exhibit strong attractive motions; the pairwise velocities depend sensitively on the model. The mean pairwise attractive cluster velocities on $5h^{-1}$ Mpc scale ranges from ~ 1700 km s^{-1} for $\Omega_m = 1$ CDM to ~ 700 km s^{-1} for $\Omega_m = 0.3$ CDM. The cluster velocity correlation function, presented in Figure 12, is negative on small scales—indicating large attractive velocities, and is positive on large scales, to $\sim 200h^{-1}$ Mpc—indicating significant bulk motions in the models. None of the models reproduce the very large bulk flow of clusters on $150h^{-1}$ Mpc scale, $v \simeq 689 \pm 178$ km s^{-1}, recently reported by Lauer and Postman (1994). The bulk flow expected on this large scale is generally $\lesssim 200$ km s^{-1} for all the models studied ($\Omega_m = 1$ and $\Omega_m \simeq 0.3$ CDM, and PBI).

12. Some Unsolved Problems

Considerable progress has been made over the last two decades in the study of clusters and superclusters of galaxies, as described in these lectures. However, many problems still remain open. I highlight some of the unsolved problems in this field that are likely to be solved in the coming decade. Currently planned large redshift surveys of galaxies and clusters such as the Sloan Digital Sky Survey and the 2dF survey, deep optical and X-ray surveys

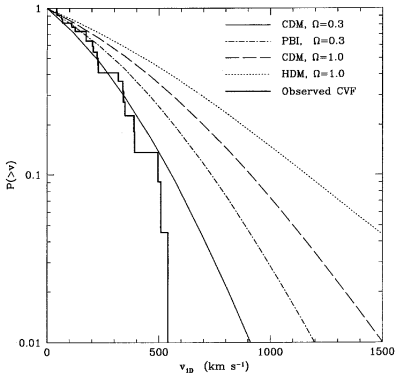

Fig. 11.— Observed vs. model cluster peculiar velocity functions (from Bahcall and Oh 1996). The Giovanelli and Haynes (1996) data are compared with model expectations convolved with the observational errors. Note the absence of a high velocity tail in the observed cluster velocity function.

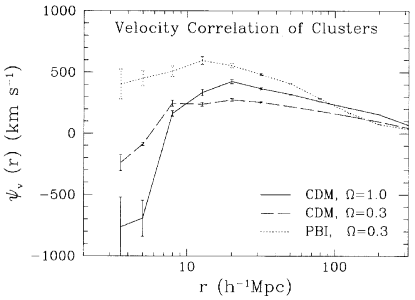

Fig. 12.— Velocity correlation function of rich ($R \geq 1$) clusters of galaxies for three models. Error bars indicate the 1σ statistical uncertainties (from Cen et al. 1994).

using HST, Keck, ROSAT, ASCA, and AXAF, among other, should allow a considerable increase in our understanding of the nature and evolution of these fundamental systems. At the same time, state of the art cosmological simulations to be available in the next decade (e.g., Ostriker, this book) should greatly enhance our ability to compare the observations with detailed expectations from various cosmologies and hopefully narrow down the correct cosmological model of our universe.

Here is a partial list of some of the interesting unsolved problems in the field of clusters and superclusters of galaxies.

Clusters of Galaxies

- What is the mass distribution and its extent in clusters of galaxies? Using gravitational lensing distortions, one can determine the mass density profile, $\rho_m(r)$, and total cluster mass, $M(r)$, of clusters and compare it with the distribution of galaxies and gas for a large sample of clusters.
- Does mass follow light on these scales? If not, what is the bias factor as a function of scale, $b(r)$?
- What is the implied density parameter from clusters, $\Omega_m(r)$?
- What is the accurate baryon-fraction in clusters and groups of galaxies, as a function of scale, $\Omega_b/\Omega(r)$?
- What is the origin of the hot intracluster gas and its metallicity?
- What is the evolution of clusters in the optical and in X-rays?
- What are the cosmological implications from studies of clusters?

Superclusters

- What is, quantitatively, the morphology of superclusters and large-scale structure (superclusters, filaments, and void network)?
- What is the dependence of the superclustering properties on galaxy luminosity, surface brightness, type (E, S), and system (galaxies versus clusters)?
- What are the peculiar motions in superclusters and on large scales?

- What is the mass, and mass distribution, in superclusters and on large scales? Does mass follow light?
- What is in the "voids"?
- What is Ω_m on large scales?
- What is the baryon fraction in superclusters?
- What is the time evolution of superclusters?
- What are the constraints made by the observed superclusters and large-scale structure on cosmology and galaxy formation models?

I expect that many of these questions will be addressed and possibly solved in the coming decade.

Acknowledgments

I thank the organizers of the Jerusalem Winter School 1995, J. P. Ostriker and A. Dekel, for an outstanding, productive, and fun school. The work by N. Bahcall and collaborators is supported by NSF grant AST93-15368.

REFERENCES

Abell, G. O. 1958, ApJS, 3, 211

Arnaud, M., Hughes, J. P., Forman, W., Jones, C., Lachieze-Rey, M., Yamashita, K., & Hatusukade, I. 1992, ApJ, 390, 345

Bahcall, J. N., & Sarazin, C. 1977, ApJ, 213, L99

Bahcall, N. A. 1975, ApJ, 198, 249

Bahcall, N. A. 1977, ARA&A, 15, 505

Bahcall, N. A. 1977a, ApJ, 217, L77

Bahcall, N. A. 1977b, ApJ, 218, L93

Bahcall, N. A. 1981, ApJ, 247, 787

Bahcall, N. A. 1988, ARA&A, 26, 631

Bahcall, N. A. 1991, ApJ, 376, 43

Bahcall, N. A. 1995, in Dark Matter, AIP Conf. Proceedings 336, ed. S. Holt and C. Bennet (New York: AIP), 201

Bahcall, N. A. 1996, in Astrophysical Quantities, ed. A. Cox (New York: AIP)

Bahcall, N. A., & Burgett, W. 1986, ApJL, 300, L35

Bahcall, N. A., & Cen, R. 1992, ApJ, 398, L81

Bahcall, N. A., & Cen, R. 1993, ApJ, 407, L49

Bahcall, N. A., & Cen, R. Y. 1994, ApJ, 426, L15

Bahcall, N. A., & Chokshi, A. 1991, ApJ, 380, L9

Bahcall, N. A., & Chokshi, A. 1992, ApJL, 385, L33

Bahcall, N. A., Gramann, M., & Cen, R. 1994, ApJ, 436, 23.

Bahcall, N. A., & Lubin, L. M. 1994, ApJ, 426, 513

Bahcall, N. A., Lubin, L M., & Dorman, V. 1995, ApJ, 447, L81

Bahcall, N. A., Miller, N., & Udomprasert, P. 1996, in preparation

Bahcall, N. A., & Oh, P. 1996, ApJ, 462, L43

Bahcall, N. A., & Soneira, R. M. 1983, ApJ, 270, 20

Bahcall, N. A,. & Soneira, R.M., 1984, ApJ, 277, 27

Bahcall, N. A., & West, M. 1992, ApJL, 392, 419

Bautz, L. P., & Morgan, W. W. 1970, ApJ, 162, L149

Birkinshaw, M., Gull, S. F., & Hardebeck, H. E. 1984, Nature, 309, 34

Broadhurst, T. J., Ellis, R., Koo, D., & Szalay, A. 1990, Nature, 343, 726

Burg, R., Giacconi, R., Forman, W., Jones, C. 1994, ApJ, 422, 37

Cen, R., Bahcall, N. A., & Gramann, M. 1994, ApJ, 437, L51

Chincarini, G., Rood, H. J., & Thompson, L. A. 1981, ApJ, 249, L47

Cole, S., Fisher, K. B., & Weinberg, D. H. 1994, MNRAS, 267, 785

da Costa, L. N., et al. 1988, ApJ, 327, 544

Dalton, G. B., Efstathiou, G., Maddox, S. J., & Sutherland, W. 1992, ApJ, 390, L1

David, L. P., Slyz, A., Jones, C., Forman, W., Vrtilek, S., & Arnaud, K. 1993, ApJ, 412, 479

de Lapparent, V., Geller, M., & Huchra, J. 1986, ApJ, 302, L1

Dekel, A. 1994, ARA&A, 32, 371

Dressler, A. 1978, Ap.J, 226, 55

Dressler, A. 1980, ApJ, 236, 351

Dressler, A. 1984, ARA&A, 22, 185

Edge, A., & Stewart, G. C., 1991, MNRAS, 252, 428

Edge, A., Stewart, G. C., Fabian, A. C., & Arnaud, K. A. 1990, MNRAS, 245, 559

Ellingson, E., Yee, H. K. C., & Green, R. F. 1991, ApJ, 371, 45

Evrard, A. E. 1990, ApJ, 363, 349

Fabian, A. C. 1992, in Clusters and Superclusters of Galaxies, NATO ASI Series No. 366, edited by A. C. Fabian (Dordrecht: Kluwer Academic), p.151

Geller, M. J. 1990, in Clusters of Galaxies, STScI Symposium No. 4, ed. W. R. Oegerle et al. (Cambridge: Cambridge Univerity Press), p. 25

Giovanelli, R., & Haynes, M. 1996, in preparation

Giovanelli, R., Haynes, M., & Chincarini, G. 1986, ApJ, 300, 77

Gregory, S. A., & Thompson, L. A. 1978, ApJ, 222, 784

Gregory, S. A., Thompson, L. A., & Tifft, W. 1981, ApJ, 243, 411

Henry, J. P., & Arnaud, K. A. 1991, ApJ, 372, 410

Henry, J. P., Gioia, I. M., Maccacaro, T., Morris, S. L., Stocke, J. T., & Walter, A. 1992, ApJ, 386, 408

Herbig, T., Lawrence, C. R., Readhead, A. C. S., & Gulkis, S. 1995, ApJL, 449, L1

Hoessel, J. G., Gunn, J. E., & Thuan, T. X. 1980, ApJ, 241, 486

Hughes, J. P. 1989, ApJ, 337, 21

Jones, C., & Forman, W. 1984, ApJ, 276, 38

Jones, C., & Forman, W. 1992, in Clusters and Superclusters of Galaxies, NATO ASI Series, No. 366, ed. A. C. Fabian (Dordrecht: Kluwer Academic), p. 49

Jones, M., Saunders, R., Alexander, P., Birkinshaw, M., & Dillon, N. 1993, Nature, 365, 320

Kaiser, N., & Squires, G. 1993, ApJ, 404, 441

King, I. 1972, ApJL, 174, L123

Landy, S., Shectman, S., Lin, H., Kirshner, R., Oemler, A., & Tucker, A. 1996, ApJ, 456, L1

Lauer, T., & Postman, M. 1994, ApJ., 425, 418

Lilje, P. B., & Efstathiou, G. 1988, MNRAS, 231, 635

Lubin, L., & Bahcall, N. A. 1993, ApJL, 415, L17

Lubin, L., Cen, R., Bahcall, N. A., & Ostriker, J. P. 1996, ApJ, 460, 10

Lumsden, S. L., Nichol, R. C., Collins, C. A., & Guzzo, L. 1992, MNRAS, 258, 1

Mushotzky, R. 1996, preprint

Nichol, R., Collins, C. A., Guzzo, L., & Lumsden, S. L. 1992, MNRAS,255, 21p

Oemler, A. 1974, ApJ, 194, 1

Oort, J. 1983, ARA&A, 21, 373

Ostriker, J. P., Peebles, P. J. E., & Yahil, A. 1974, ApJ, 193, L1

Peacock, J., & West, M. 1992, MNRAS, 259, 494

Peebles, P. J. E. 1980, The Large Scale Structure of the Universe (Princeton: Princeton University Press)

Peebles, P. J. E. 1993, Principles of Physical Cosmology (Princeton: Princeton University Press)

Postman, M., & Geller, M. 1984, ApJ, 281, 95

Romer, A.K., Collins, C., Böhringer, H., Cruddace, R., Ebeling, H., MacGillivray, H., & Voges, W. 1994, Nature, 372, 75

Rood, H. J. 1988, ARA&A, 26, 245

Rood, H. J., & Sastry, G. N. 1971, PASP, 83, 313

Sarazin, C. L. 1986, Rev. Mod. Phys., 58, 1

Schechter, P. L. 1976, ApJ, 203, 297

Shaver, P. 1988, in Large-Scale Structure of the Universe, IAU Symposium No. 130, ed. J. Audouze et al. (Dordrecht: Reidel), 359

Shectman, S., Landy, S., Oemler, A., Tucker, A., Lin, H., & Kirshner, R. 1996, ApJ, in press (preprint astro-ph/9604167)

Smail, J., Ellis, R., Fitchett, M., & Edge, A. 1995, MNRAS, 273, 277

Strauss, M., & Willick, J. 1995, Phys. Reports, 261, 271

Struble, M., & Rood, H. 1991, ApJS, 77, 363

Sunyaev, R. A., & Zeldovich, Ya. B., 1972, Comments Astrophys. Space Phys., 4, 173

Szalay, A., & Schramm, D. N. 1985, Nature, 314, 718

Tyson, J. A., & Fischer, P. 1996, ApJL, in press

Tyson, J. A., Valdes, F., & Wenk, R. A. 1990, ApJ, 349, Ll

Walker, T. P., et al. 1991, ApJ, 376, 51

White, D., & Fabian, A. 1995, MNRAS, 273, 72

White, S. D. M., Navaro, J. F., Evrard, A. E., & Frenk, C. S. 1993 Nature, 366, 429

Wilbanks, T. M., Ade, P. A. R., Fischer, M. L., Holzapfel, W. L., & Lange, A. 1994, ApJ, 427, L75

Yee, H. K. C. 1992, in Clusters and Superclusters of Galaxies, NATO ASI Series No. 366, ed. A. C. Fabian (Dordrecht: Kluwer Academic), 293

Yee, H. K. C., & Green, R. F. 1987, ApJ, 319, 28

Zwicky, F. 1957, Morphological Astronomy (Berlin: Springer)

This preprint was prepared with the AAS LaTeX macros v4.0.